Acta Crystallographica Section B
Structural Science
ISSN 0108-7681

$SiBr_4$ – prediction and determination of crystal structures

Alexandra K. Wolf,[a] Jürgen Glinnemann,[a] Martin U. Schmidt,[a]* Jianwei Tong,[b] Robert E. Dinnebier,[b] Arndt Simon[b] and Jürgen Köhler[b]

[a]Goethe University, Institute of Inorganic and Analytical Chemistry, Max-von-Laue-Strasse 7, 60438 Frankfurt am Main, Germany, and [b]MPI for Solid State Research, Heisenbergstrasse 1, 70569 Stuttgart, Germany

Correspondence e-mail: m.schmidt@chemie.uni-frankfurt.de

Received 13 February 2009
Accepted 31 March 2009

For $SiBr_4$ no crystal structures have been reported yet. In this work the crystal structures of $SiBr_4$ were predicted by global lattice-energy minimizations using force-field methods. Over an energy range of 5 kJ mol^{-1} above the global minimum ten possible structures were found. Two of these structures were experimentally determined from X-ray synchrotron powder diffraction data: The low-temperature β phase crystallizes in $P2_1/c$, the high-temperature α phase in $Pa\overline{3}$. Temperature-dependant X-ray powder diffraction shows that the phase transition occurs at 168 K.

1. Introduction

$SiBr_4$ (mp 278 K) is the only tetrahedral EX_4 compound (E = C, Si, Ge, Sn, Pb; X = F, Cl, Br, I) for which no crystal structure has yet been reported (see Table 1). This is all the more astonishing because in 1931 Pohland described two modifications of $SiBr_4$ (Pohland, 1931); by polarization–microscopy analysis one modification ($T < 243$ K) was assigned to the tetragonal crystal system, the other, obtained at higher temperature, to the cubic crystal system.

The structures, configurations and bond lengths of a number of EX_4 molecules in the gas phase have been investigated *via* scattering of fast electrons (Lister & Sutton, 1941). Shortly after that Spitzer *et al.* (1943) used the same technique to study the structure of $SiBr_4$, which confirmed the previous results. Recently, some elastic and rotationally inelastic cross-section calculations by low-energy electron scattering of several tetrahalides have been reported by Varella *et al.* (1999).

Earlier packing analyses of EX_4 compounds (Wolf *et al.*, 2008) showed that in all structures the molecules (and thus the E atoms) form distorted sphere packings, including hexagonal close packing (h.c.p.), cubic close packing (c.c.p.), body-centered cubic (b.c.c. – W structure) and cubic primitive packing (c.p. – Po structure). Furthermore, a packing(s) similar to the S atoms in pyrite (FeS_2) or the O atoms in solid CO_2 (Mark & Pohland, 1926; Simon & Peters, 1980) is observed. The X atoms also adopt distorted close-packing arrangements (c.c.p., h.c.p., b.c.c. or c.p.). Altogether seven different structure types can be described; each structure type corresponds to a specific combination of space group and number of formulae in the unit cell, Z (Table 2; Wolf *et al.*, 2008).

Here we present a full crystal-structure prediction of $SiBr_4$ by lattice-energy minimizations. Independently the structures of two polymorphs of $SiBr_4$ were determined from X-ray synchrotron powder diffraction data.

The halogen–halogen interactions of the experimental and calculated structures, as well as the structure types, are described.

Table 1
Space groups and number of molecules per unit cell of published experimental crystal structures of molecular EX_4 compounds (after Wolf *et al.*, 2008).

E/*X*	F	Cl	Br	I
C	$C2/c$; $Z = 4$[a]	$P2_1/c$; $Z = 4$[b] $C2/c$; $Z = 32$[e]†	$C2/c$; $Z = 32$[c]†	$I\bar{4}2m$; $Z = 2$[d]
Si	$I\bar{4}3m$; $Z = 2$[f]	$P2_1/c$; $Z = 4$[g]	No structure published	$Pa\bar{3}$; $Z = 8$[h]
Ge	$I\bar{4}3m$; $Z = 2$[i]	$P2_1/c$; $Z = 4$[j]	$Pa\bar{3}$; $Z = 8$[k] $P2_1/c$; $Z = 4$[m]	$Pa\bar{3}$; $Z = 8$[l]
Sn	Octahedral coordination of Sn[n]	$P2_1/c$; $Z = 4$[o]	$P2_1/c$; $Z = 4$[p]	$Pa\bar{3}$; $Z = 8$[q] $P\bar{4}3m$; $Z = 1$[r]
Pb	Octahedral coordination of Pb[n]	$C2/c$; $Z = 4$[s]	Unstable[t]	Unstable[t]

(*a*) Bol'shutkin *et al.* (1972), Peþe & Gay (1989), Fitch & Cockcroft (1993); (*b*) Piermarini & Braun (1973); (*c*) Lindeman *et al.* (2003); (*d*) Pohl (1982); (*e*) Cohen *et al.* (1979); (*f*) Atoji & Libscomb (1954); (*g*) Zakharov *et al.* (1986); (*h*) Biehl & Schubert (2000); (*i*) Köhler *et al.* (1988); (*j*) Merz & Driess (2002); (*k*) Köhler, Okudera, Reuter & Simon (2005); (*l*) Walz *et al.* (1993); (*m*) Köhler, Okudera & Simon (2005); (*n*) Bork & Hoppe (1996); (*o*) Reuter & Pawlak (2000); (*p*) Reuter & Pawlak (2001); (*q*) Burrow (2005); (*r*) Ott (1926); (*s*) Maley *et al.* (2002); (*t*) Huber (1967). † High pressure.

Table 2
Structure types for published EX_4 compounds (after Wolf *et al.*, 2008).

Space group	*Z*	Site symmetry of molecule	Arrangement of the molecules/ Arrangement of *X* atoms
$I\bar{4}3m$	2	$\bar{4}3m$	b.c.c./c.p.
$P\bar{4}3m$	1	$\bar{4}3m$	c.p./c.c.p.
$I\bar{4}2m$	2	$\bar{4}2m$	c.c.p./b.c.c.
$Pa\bar{3}$	8	3	s/c.c.p.
$C2/c$	4	2	c.c.p./c.c.p.
$P2_1/c$	4	1	h.c.p./h.c.p.
$C2/c$	32	All 1	c.c.p./'h.c.p.'

Abbreviations for (distorted) structure types: c.c.p. – cubic close packing; h.c.p. – hexagonal close packing; b.c.c. – body-centred cubic packing as in W; c.p. – cubic primitive as in Po; s – like sulfur partial structure in pyrite (FeS_2); 'h.c.p.' – an intergrowth of mainly h.c.p. with c.c.p.

2. Crystal-structure prediction

2.1. Computations

The crystal structures of $SiBr_4$ were predicted using the program *CRYSCA* (Schmidt & Kalkhof, 1997) by global minimization of the lattice energy. In *CRYSCA* the energy is described as the sum of van der Waals and electrostatic terms. The van der Waals energy E_{vdW} is calculated by

$$E_{vdW} = \frac{1}{2}\sum_i \sum_j (-A_{ij} r_{ij}^{-6} + B_{ij} e^{-C_{ij} r_{ij}}), \quad (1)$$

where r_{ij} is interatomic distance between atoms *i* and *j*; *i*: all atoms of a given molecule; *j*: all atoms of all other molecules; A_{ij}, B_{ij}, C_{ij}: empirical potential parameters.

The van der Waals energy is summed up with a cut-off radius of 20 Å.

In the first calculations the van der Waals parameters (A_{ij}, B_{ij}, C_{ij}) for bromine were taken from the Dreiding parametrization (Mayo *et al.*, 1990). As a test, possible crystal structures for $GeBr_4$ were calculated and the results compared with the two experimental structures (Köhler, Okudera, Reuter & Simon, 2005; Köhler, Okudera & Simon, 2005). The experimental crystal structures could be found in the list of low-energy structures, but the calculated lattice parameters were too small. Thus, the van der Waals parameters for bromine were modified. The Br···Br potential was changed by increasing r_{min} from 3.9442 to 4.2442 Å. The depth of the potential, $E(r_{min})$, as well as the steepness, λ, remained unchanged. Mixed Ge ··· Br parameters were calculated using the combination rules (Mirskaya, 1973).

Table 3
Experimental and calculated lattice parameters of $GeBr_4$.

	Experimental	Calculated	Difference (%)
$Pa\bar{3}$, $T = 213$ K			
a (Å)	11.1723 (1)	11.173	0.006
$P2_1/c$ $T = 93$ K			
a (Å)	10.183 (2)	10.225	0.412
b (Å)	6.779 (1)	6.794	0.221
c (Å)	10.292 (2)	10.238	−0.525
β (°)	102.54 (3)	101.36	−1.151

Table 4
van der Waals potential parameters [see (1)].

	A (kJ Å^6 mol^{-1})	*B* (kJ mol^{-1})	*C* (Å^{-1})
Si···Si	10 954	2 720 898	3.460
Si···Br	14 141	827 966	3.143
Br···Br	18 256	251 949	2.825

$$A_{ij} = (A_{ii} \cdot A_{jj})^{1/2} \quad (2)$$

$$B_{ij} = (B_{ii} \cdot B_{jj})^{1/2} \quad (3)$$

$$C_{ij} = \frac{1}{2}(C_{ii} + C_{jj}) \quad (4)$$

Using these parameters the experimental crystal structures of $GeBr_4$ could be reproduced with high accuracy. The experimental and calculated lattice parameters for $GeBr_4$ are given in Table 3. All deviations are within experimental error.

For $SiBr_4$ the parameters for bromine were the adjusted ones. The van der Waals parameters for silicon were taken from Schmidt (1994). Mixed Si···Br parameters were calculated using the combination rules [see (2), (3) and (4)]. The resulting van der Waals parameters for $SiBr_4$ are given in Table 4.

For the electrostatic energy E_{es} the Coulomb summation was used

$$E_{es} = \frac{1}{2}\sum_i \sum_j \frac{1}{4\pi\epsilon_r\epsilon_0} \cdot \frac{q_i q_j}{r_{ij}}. \quad (5)$$

Point charges q_i, q_j were assigned to the atomic centres. The charges were calculated using the electrostatic potential (ESP) method within the MNDO approach. The relative permittivity ϵ_r was set to the vacuum value ($\epsilon_r = 1$).

Table 5
Low-energy crystal structures of $SiBr_4$ calculated by lattice-energy minimizations.

Rank	Energy (kJ mol^{-1})	Space group	Z	Site symmetry of molecule	a (Å)	b (Å)	c (Å)	β (°)
1	−254.228	$C2/c$	4	2	12.314	5.662	11.173	116.86
2	−253.951	$Pbcn$	4	2	5.660	11.149	11.014	
3	−253.440	$Pbca$	8	1	5.667	11.124	22.052	
4	−252.880	$P2_1/c$	4	1	10.217	6.799	10.226	101.45
5	−252.609	$I\bar{4}2m$	2	$\bar{4}2m$	5.659		10.873	
6	−252.548	$P4_2/nmc$	2	$\bar{4}m2$	7.833		5.666	
7	−252.111	$Pmn2_1$	2	m	7.931	6.798	6.464	
8	−251.278	$Pnma$	4	m	13.595	7.941	6.459	
9	−251.268	$Pa\bar{3}$	8	3	11.167			
10	−250.434	$Pbcn$	4	2	5.635	21.899	5.645	

The summation for the electrostatic energy included 5 × 5 × 5 unit cells.

All calculations were carried out with one complete molecule in the asymmetric unit. The molecular geometry of $SiBr_4$ was constructed with full tetrahedral symmetry ($\bar{4}3m$). The Si—Br bond length of the model was based on the results of searches of the databases CSD (Allen, 2002) and ICSD (Belsky *et al.*, 2002) for compounds with tetrahedrally coordinated silicon bonded to at least one bromine atom. This resulted in a mean bond length of 2.250 Å.

For the lattice-energy calculations statistically frequent space groups for molecular compounds were used [$P\bar{1}$ ($Z = 2$), $P2_1$ ($Z = 2$), Cc ($Z = 4$), $P2_1/c$ ($Z = 4$), $P2_12_12_1$ ($Z = 4$), $Pna2_1$ ($Z = 4$), $Pca2_1$ ($Z = 4$), $Pbca$ ($Z = 8$) and $P1$ ($Z = 1$)]. Since the molecule itself is highly symmetrical, various supergroups may be reached. The minimizations started from a set of 10 000–100 000 different structures with random starting values for the lattice parameters, and for the position and the orientation of the molecule. The molecular structure was kept fixed with the point group $\bar{4}3m$.

The minima were sorted according to energy. All low-energy structures were found several times, from different starting values, indicating that the calculations were complete and no low-energy structures were missing.

To account for molecular flexibility all low-energy structures (excluding duplicates) were post-optimized using the program package *Cerius*[2] (Accelrys, 2003) with the Dreiding 2.21 force field (Mayo *et al.*, 1990). The van der Waals parameters for bromine were the same as for the *CRYSCA* calculations, whereas the parameters for silicon were slightly different. The resulting differences can be neglected, because silicon is surrounded by bromine and there are no close intermolecular interactions involving Si atoms. During this post-optimization the geometry of the molecule, its position and orientation, and the lattice parameters were optimized simultaneously. All structures were inspected for higher symmetry, and if necessary, transformed to the corresponding supergroups.

2.2. Results

In an energy range of 5 kJ mol^{-1} ten low-energy crystal structures were found (Table 5). Thus, these are potential polymorphs. The energetically best crystal structure is found in $C2/c$, $Z = 4$, with the molecule on a twofold axis (Table 5, Fig. 1). In this structure the Br atoms form a distorted cubic close packing, with the Si atoms occupying 1/8 of the tetrahedral voids in such a way that the molecules themselves also form a distorted cubic close packing. This structure type is also found experimentally for CF_4 and $PbCl_4$ (Tables 1 and 2). In the other low-energy structures the Br atoms adopt various sphere packings.

From the seven structure types observed experimentally for other EX_4 compounds (Table 2) four could be found for $SiBr_4$ in the calculations ($C2/c$, $Z = 4$, c.c.p. for E, c.c.p. for X; $I\bar{4}2m$, $Z = 2$, c.c.p. for E, b.c.c. for X; $P2_1/c$, $Z = 4$, h.c.p. for E, h.c.p. for X; $Pa\bar{3}$, $Z = 8$, s for E, c.c.p. for X). Two of them were verified experimentally (§§3 and 4). Three of the seven structure types ($C2/c$, $Z = 32$, $P\bar{4}3m$, $Z = 1$ and $I\bar{4}3m$, $Z = 2$) are energetically unfavourable for $SiBr_4$.

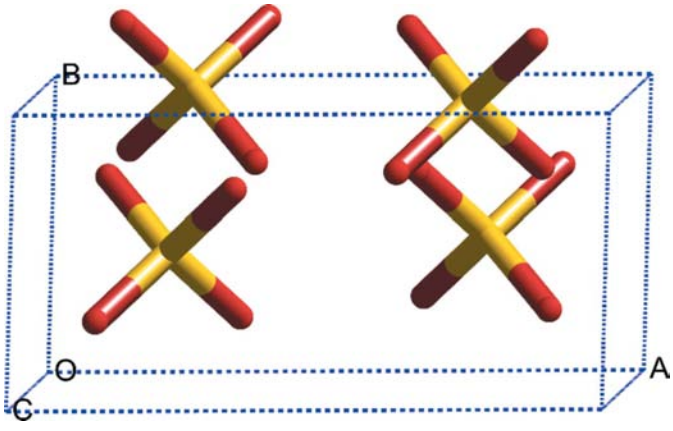

Figure 1
Calculated lowest-energy structure for $SiBr_4$ ($C2/c$, $Z = 4$).

3. X-ray powder diffraction

In situ X-ray powder diffraction data of $SiBr_4$ were collected at low temperatures in Debye–Scherrer geometry with a Cryostream 600 cold-air blower (Oxford Cryosystems) on a motorized goniometer head at beamline X7B at the National Synchrotron Light Source (NSLS) at Brookhaven National Laboratory. X-rays of energy 13.5 keV were selected by a double flat-crystal monochromator in an ultra-high vacuum located 8 m from the source. The size of the beam was adjusted to a size of approximately 0.5 mm^2. The detector, a MAR 345 image-plate reader, was set up perpendicular to the beam path at a distance of approximately 227 mm from the

sample. LaB_6 was used as an external standard to determine the beam center, sample-to-detector distance, exact wavelength ($\lambda = 0.92103$ Å), and tilting angle of the image plate. The sample was contained in a sealed lithium borate glass capillary with 0.5 mm diameter. The sample was aligned such that it was close to the centre of the nozzle of the cold-air blower at a distance of approximately 5 mm. The sample was shock-cooled to $T = 120$ K and slowly reheated back to room temperature ($T = 280$ K) in 70 min. During exposure, the sample was rocked by 60° in order to improve randomization of the crystallites. An exposure time of 60 s was chosen to match the saturation intensity of the image plate. Together with a readout time of 80 s of the image plate reader, this led to a heating rate of 5.33 K per scan. Integration of the full-circle powder patterns were performed using the program *FIT2D* (Hammersley *et al.*, 1996) resulting in diagrams of corrected intensities *versus* the scattering angle 2θ (Fig. 2). The diffracted intensity distribution over the Debye–Scherrer rings indicated the presence of severe texture.

Attempts were made to grow single crystals of $SiBr_4$ in a capillary (0.2 mm diameter) on a four-circle diffractometer. However, no crystal was obtained because of extreme supercooling of the $SiBr_4$ liquid below its equilibrium melting point of 278 K. The sudden freezing that occurred at temperatures below 250 K led to microcrystallinity, and all efforts to grow larger species failed.

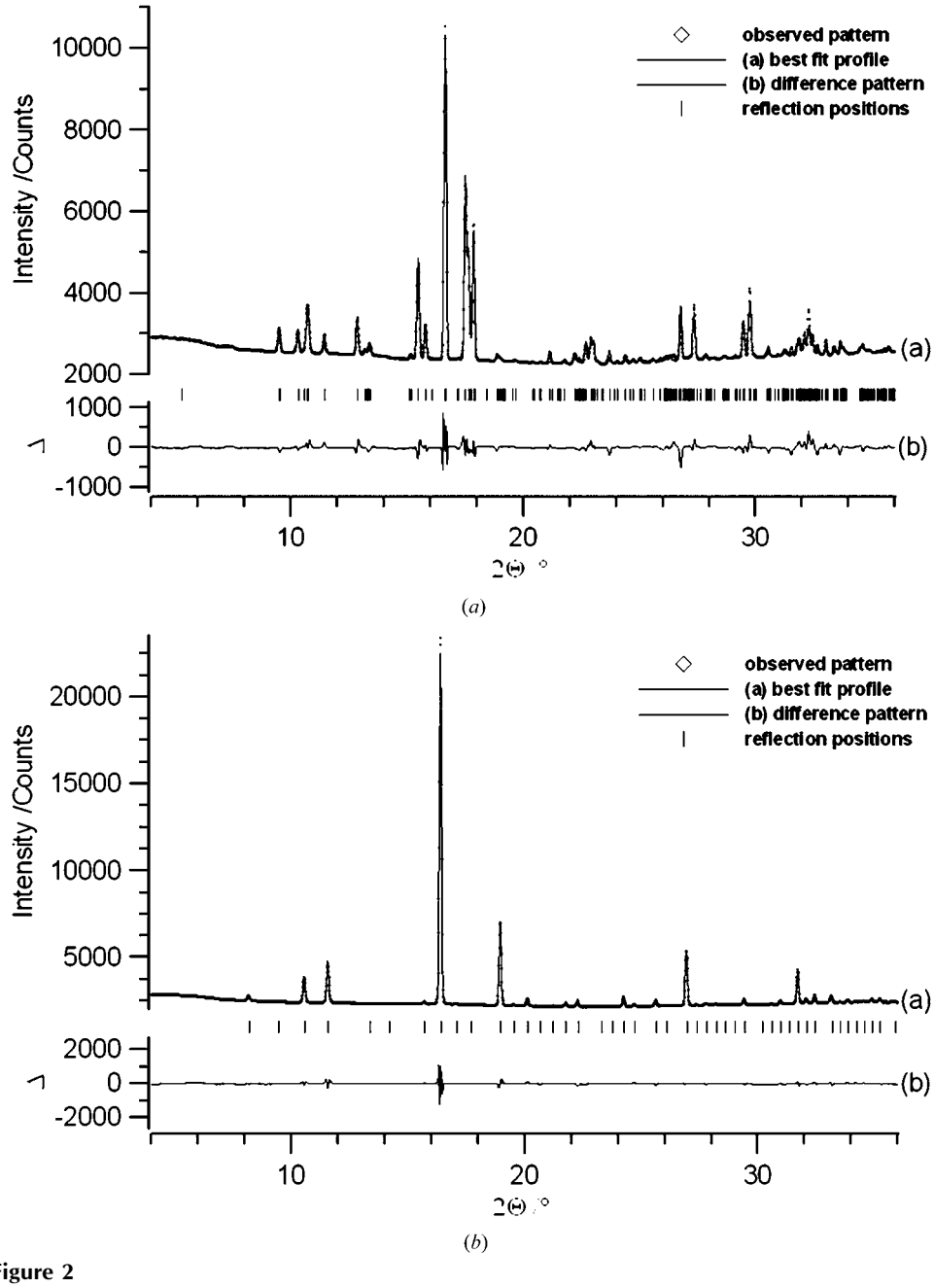

Figure 2
Rietveld plot (*a*) for β-$SiBr_4$ at $T = 147$ K and (*b*) for α-$SiBr_4$ at $T = 237$ K. The wavelength was $\lambda = 0.92103$ Å.

4. Structure solution and refinement

A presentation of the observed scattered X-ray intensities for $SiBr_4$ as a function of temperature is shown in Fig. 3. A sharp phase transition from the low-temperature β phase to the high-temperature α phase could be observed at $T = 168$ K. Due to a heating rate of 2.28 K min^{-1}, the phase transition is completed around 175 K.

For indexing the powder pattern of β-$SiBr_4$ at $T = 147$ K, the program *TOPAS* (Bruker, 2000) was used. Indexing was performed by iterative use of singular value decomposition (LSI; Coelho, 2003), leading to a primitive monoclinic unit cell with lattice parameters given in Table 6. The most probable space group was determined to be $P2_1/c$ from the observed reflection conditions (Köhler, Okudera & Simon, 2005). The number of formula units per unit cell was determined to be $Z = 4$ from volume increments.

The crystal structure of β-$SiBr_4$ at $T = 147$ K was solved by the global optimization method of simulated annealing in real space using the *TOPAS* program. The peak profiles and precise lattice parameters of the powder pattern of β-$SiBr_4$ at $T = 147$ K were first determined by a LeBail fit (LeBail *et*

Table 6
Crystallographic data for the high- and low-temperature phases of $SiBr_4$.

	α-$SiBr_4$	β-$SiBr_4$
Temperature (K)	237	147
Formula weight (g mol^{-1})	347.69	347.69
Space group (No.)	$Pa\overline{3}$ (205)	$P2_1/c$ (14)
Z	8	4
a (Å)	11.1770 (1)	10.1319 (4)
b (Å)		6.7002 (2)
c (Å)		10.2389 (3)
β (°)		102.66 (1)
V (Å^3)	1396.3 (1)	678.2 (1)
ρ_{calc} (g cm^{-3})	3.308 (1)	3.406 (1)
Wavelength (Å)	0.92103	0.92103
R_{exp}†	0.020	0.019
R_p†	0.010	0.013
R_{wp}†	0.017	0.023
R_{F^2}†	0.006	0.025
Starting angle (°2θ)	4	4
Final angle (°2θ)	36	36
Step width (°2θ)	0.02	0.02
Time/scan (s)	140	140
No. of variables	25	49

† R_{exp}, R_p, R_{wp} and R_{F^2} as defined in *TOPAS* (Bruker, 2000).

al., 1988) using the fundamental parameter (FP) approach of *TOPAS* (Cheary *et al.*, 2005). A good fit to the data was obtained. The tetrahedral $SiBr_4$ molecule was constructed with the aid of the rigid-body editor of *TOPAS* using standard bond lengths and angles (Kratky *et al.*, 1985). To solve the crystal structure of β-$SiBr_4$, six external degrees of freedom were subjected to global optimization: three translations and three rotations. The average Si—Br bond length of the β-$SiBr_4$ molecule was included in the structure-determination process as an internal degree of freedom. The structure giving the best fit to the data in the space group $P2_1/c$ was validated by Rietveld refinement using the *TOPAS* program. The apparent texture was successfully modelled using symmetrized spherical harmonics of fourth order. An overall isotropic atomic displacement parameter for the $SiBr_4$ molecule was refined. For β-$SiBr_4$ at $T = 147$ K, the final Rietveld plot is given in Fig. 2(*a*), and final agreement factors are listed in Table 6. The unit cell is shown in Fig. 4. Each Si—Br bond length was refined to the same value of 2.175 (3) Å, and each Br—Si—Br angle was fixed at 109.47°.

Starting values for the Rietveld refinement of the highly rotationally disordered high-temperature α phase of $SiBr_4$ in space group $Pa\overline{3}$ at $T = 237$ K were taken from the structure of $GeBr_4$ (Köhler, Okudera, Reuter & Simon, 2005). The apparent pronounced texture was successfully modelled using symmetrized spherical harmonics of eighth order. An overall isotropic atomic displacement parameter for the $SiBr_4$ molecule was refined. A typical Rietveld plot is given in Fig. 2(*b*), and final agreement factors are listed in Table 6. The high degree of rotational disorder is also visible as a strongly increased hump in the background compared with the low-temperature phase. The unit cell is shown in Fig. 5. A selection of intramolecular distances and angles is given in Table 7.

The dependence of the crystal structure of $SiBr_4$ on temperature was analysed by performing LeBail refinements on the 24 datasets of starting from $T = 120$ K up to $T = 242$ K. The dependence of the lattice parameters and the volume on temperature is shown in Fig. 3.

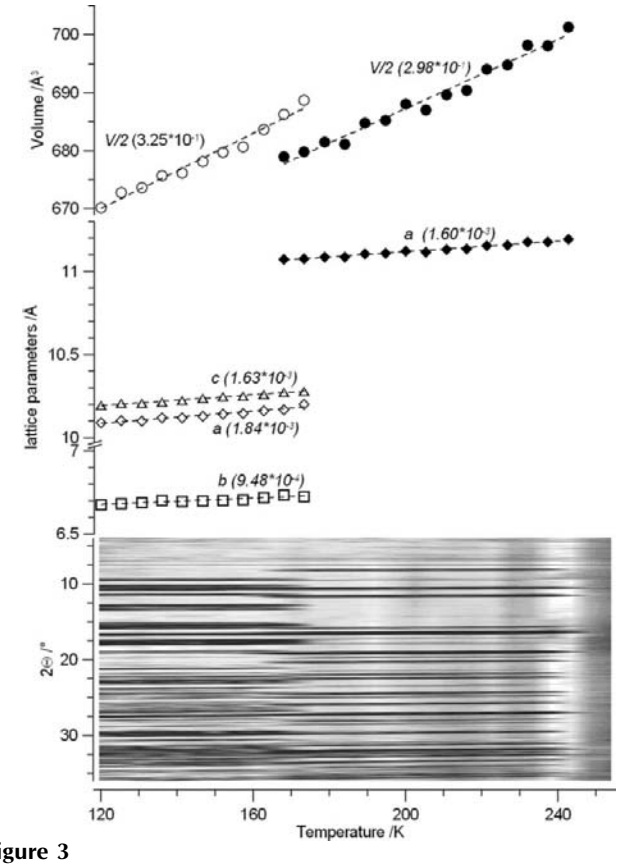

Figure 3
Cell volume (top), lattice parameters (middle) and powder diffraction patterns (bottom) of $SiBr_4$ as a function of temperature in the range from $T = 120$ K up to $T = 242$ K (2.28 K min^{-1}). The phase transition at $T = 168$ K is clearly visible. The value in parenthesis is the expansion coefficient of the corresponding parameter in Å K^{-1} for a, b and c, and in Å^3 K^{-1} for volume, which was determined by a linear fit.

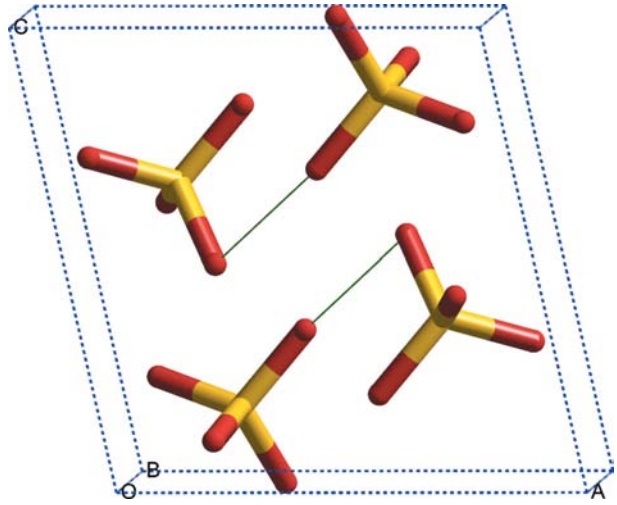

Figure 4
Experimental structure of β-$SiBr_4$ at $T = 147$ K in $P2_1/c$, $Z = 4$. Lines: closest intermolecular halogen–halogen contacts with $3.7 < r < 4.0$ Å.

5. Discussion

The two predicted structures are very similar to the experimental ones (Table 7).

The low-temperature β phase ($P2_1/c$, $Z = 4$ – h.c.p./h.c.p.) corresponds to the predicted structure at rank 4 (Table 5). In the experimental as well as in the calculated structure, the molecule is situated on the general position. The Br atoms form a distorted hexagonal close packing with the Si atoms occupying 1/8 of the tetrahedral voids. The molecules themselves also form a distorted hexagonal close packing (Fig. 6). This structure type is also found for $GeBr_4$, $SnBr_4$ and the chlorine compounds from C to Sn (Tables 1 and 2).

In the experimental structure, two Br atoms of two different molecules form short contacts with Br···Br distances below 4 Å (Fig. 4).

The volume of the calculated structure of the β phase is 2.65% larger than the volume of the experimental structure because the calculations were effectively temperature-independent and at ambient conditions, but the volume decreases with decreasing temperature.

The high-temperature α phase ($Pa\bar{3}$, $Z = 8$ – s/c.c.p.) corresponds to the predicted structure at rank 9 (Table 5). In the experimental as well as in the calculated structure, the molecule is situated on a threefold axis. The Br atoms form a distorted cubic close packing. The occupation of the tetrahedral voids occurs in such a way that two molecules are arranged pairwise in a staggered conformation of the Br atoms with a short Si···Si distance of 5.072 Å. As mentioned above the pairs of Si atoms are packed like the S atoms in pyrite (FeS_2) or the O atoms of CO_2 in the solid (Fig. 7). α-$SiBr_4$ is isostructural to SiI_4, $GeBr_4$, GeI_4 and SnI_4 (Tables 1 and 2).

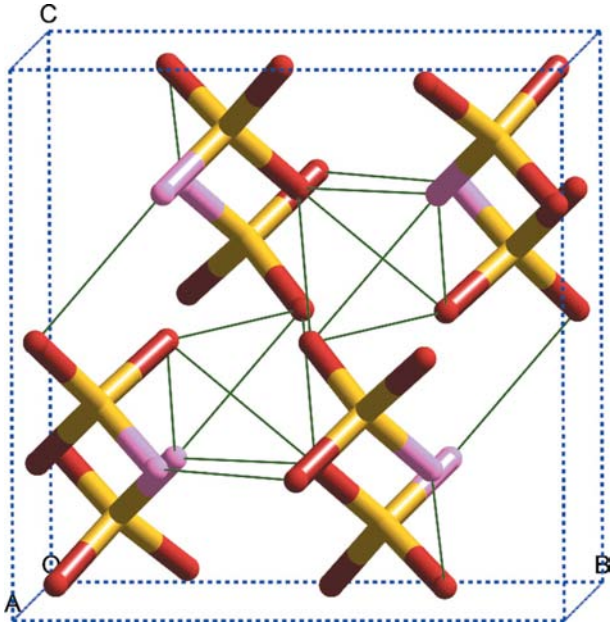

Figure 5
Experimental structure of α-$SiBr_4$ at $T = 237$ K in $Pa\bar{3}$, $Z = 8$. The representation of Br2 is darker than of Br1. Lines: closest intermolecular halogen–halogen contacts with $3.7 < r < 4.0$ Å.

Table 7
Some characteristics of the experimental and calculated crystal structures.

	Experimental	Calculated	Difference (%)
α phase: $Pa\bar{3}$, $Z = 8$ ($T = 237$ K)			
a (Å)	11.1770 (1)	11.167	−0.09
V (Å^3)	1396.3 (1)	1392.5	−0.27
Si1—Br1 (Å)	2.155 (24)	2.250	4.4
Si1—Br2 ×3 (Å)	2.201 (9)	2.250	2.2
Br1—Si1—Br2 ×3 (°)	108.46 (51)	108.83	0.34
Br2—Si1—Br2 ×3 (°)	110.47 (52)	110.10	−0.33
β phase: $P2_1/c$, $Z = 4$ ($T = 147$ K)			
a (Å)	10.139 (4)	10.217	0.77
b (Å)	6.7002 (2)	6.799	1.47
c (Å)	10.2389 (3)	10.226	−0.13
β (°)	102.66 (1)	101.45	−1.18
V (Å^3)	678.2 (1)	696.2	2.65
Si—Br (Å)	2.175 (3)	2.250	3.3
Br—Si—Br (°)	109.47†	108.74	−0.67
		108.89	−0.53
		109.31	−0.15
		109.70	0.21
		109.84	0.34
		110.33	0.79

† The Br—Si—Br angle was fixed at 109.47°.

In the experimental structure of the α phase, four Br atoms of four different molecules form short contacts *via* an empty tetrahedral void (Fig. 5).

The coordination number of the molecules increases slightly from 12 with Si···Si distances of 5.288 (1×), 5.604 (2×), 6.141 (2×), 6.519 (1×), 6.700 (2×), 6.763 (2×) and

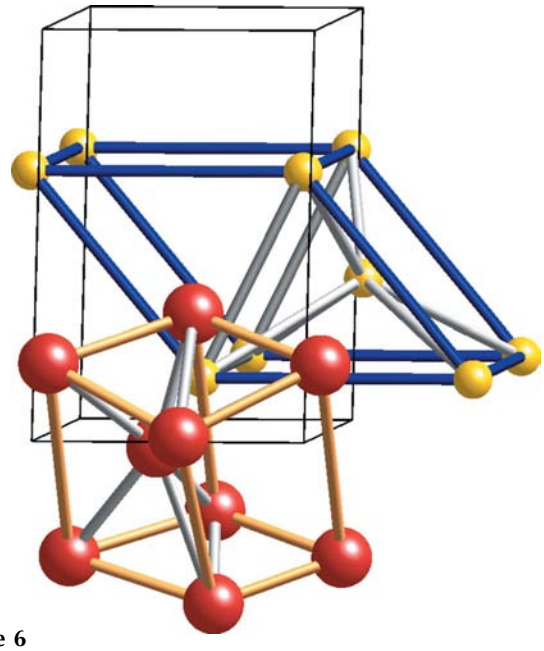

Figure 6
Structure type $P2_1/c$, $Z = 4$ – h.c.p./h.c.p. Thin black lines: edges of the unit cell of the EX_4 structure; yellow balls and blue rods: 'unit cell' of the E atoms' partial structure, a distorted hexagonal close packing (h.c.p.); red balls and yellow rods: 'unit cell' of the X atoms' partial structure, distorted h.c.p.; grey rods: guide to the eye to visualize the partial structure types. This figure is in colour in the electronic version of this paper.

6.776 Å in the low-temperature β phase to 1 + 12 with Si···Si distances of 5.072 (1×), 6.189 (6×) and 6.847 Å (6×) in the high-temperature α phase.

The differences in bond lengths and angles between the α and β phases are within the 3σ range, thus the deviations are not statistically significant and the molecules do not deviate from regular tetrahedra.

In both structures the differences between the calculated and experimental Si—Br bond lengths are well within the precision range of the experiments and calculations; the experimental Si—Br bond lengths are slightly shorter than assumed in the calculations.

6. Conclusions

By global lattice-energy minimizations ten possible crystal structures were predicted within an energy range of 5 kJ above the global minimum. Two of them were verified experimentally. The two predicted structures are very similar to the experimental ones, which could be determined from X-ray synchrotron powder diffraction data. Below 168 K $SiBr_4$ exists in a monoclinic β phase in $P2_1/c$ ($Z = 4$), which above 168 K transforms to a cubic α phase in $Pa\bar{3}$ ($Z = 8$). These two structures represent different structure types. Both phases have also been determined for $GeBr_4$, for which the phase transition occurs at approximately 213 K.

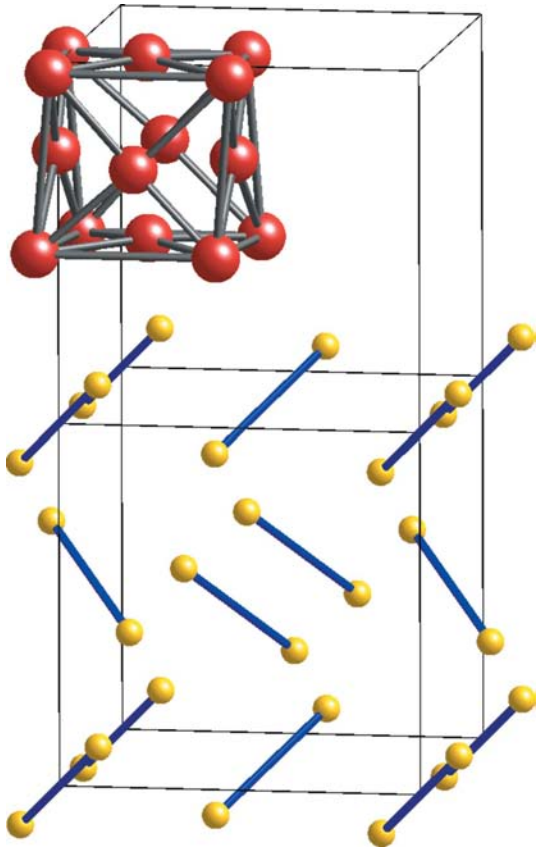

Figure 7
Structure type $Pa\bar{3}$, $Z = 8$ – s/c.c.p. Thin black lines: edges of two unit cells of the EX_4 structure; yellow balls and blue rods: the partial structure of the E atoms, like the S_2^{2-} dumbbells in the FeS_2 pyrite structure (s); red balls and grey rods: the partial structure of the X atoms, a distorted cubic close packing (c.c.p.). This figure is in colour in the electronic version of this paper.

Financial support by the Bundesministerium für Bildung und Forschung (BMBF), and the Fonds der Chemischen Industrie (FCI) is gratefully acknowledged. This work was carried out in part at the National Synchrotron Light Source at Brookhaven National Laboratory, which is supported by the US Department of Energy, Division of Materials Sciences and Division of Chemical Sciences under contract DE-AC02-98CH10886 by the US Department of Energy, Division of Chemical Sciences, Office of Basic and Energy Sciences.

References

Accelrys Ltd (2003). *Cerius*2, Version 4.9. Accelrys Ltd, Cambridge, England.
Allen, F. H. (2002). *Acta Cryst.* B**58**, 380–388.
Atoji, M. & Lipscomb, W. N. (1954). *Acta Cryst.* **7**, 597.
Belsky, A., Hellenbrandt, M., Karen, V. L. & Luksch, P. (2002). *Acta Cryst.* B**58**, 364–369.
Biehl, E. & Schubert, U. (2000). *Monatsh. Chem.* **131**, 813–818.
Bol'shutkin, D. N., Gasan, V. M., Prokhvatilov, A. I. & Erenburg, A. I. (1972). *Acta Cryst.* B**28**, 3542–3547.
Bork, M. & Hoppe, R. (1996). *Z. Anorg. Allg. Chem.* **622**, 1557–1563.
Bruker (2000). *TOPAS*, Version 2.0. Bruker AXS, Karlsruhe, Germany.
Burrow, R. A. (2005). ICSD 415735.
Cheary, R. W., Coelho, A. A. & Cline, J. P. (2005). *J. Res. Natl. Inst. Stand. Technol.* **109**, 1–25.
Coelho, A. A. (2003). *J. Appl. Cryst.* **36**, 86–95.
Cohen, S., Powers, R. & Rudman, R. (1979). *Acta Cryst.* B**35**, 1670–1674.
Fitch, A. N. & Cockcroft, J. K. (1993). *Z. Kristallogr.* **203**, 29–39.
Hammersley, A. P., Svenson, S. O., Hanfland, M. & Hauserman, D. (1996). *High Press. Res.* **14**, 235.
Huber, F. (1967). *Angew. Chem. Int. Ed. Eng.* **6**, 572.
Köhler, J., Okudera, H., Reuter, D. & Simon, A. (2005). *Z. Kristallogr.* **220**, 523.
Köhler, J., Okudera, H. & Simon, A. (2005). *Z. Kristallogr.* **220**, 524.
Köhler, J., Simon, A. & Hoppe, R. (1988). *J. Less-Common Met.* **137**, 333–341.
Kratky, Ch., Hengge, H., Stüger, H. & Rheingold, A. L. (1985). *Acta Cryst.* C**41**, 824–827.
LeBail, A., Duroy, H. & Fourquet, J. L. (1988). *Mater. Res. Bull.* **23**, 447–452.
Lindeman, S. V., Hecht, J. & Kochi, J. K. (2003). *J. Am. Chem. Soc.* **125**, 11597–11606.
Lister, M. W. & Sutton, L. E. (1941). *Trans. Farad. Soc.* **37**, 393–406.
Maley, I. J., Parsons, S. & Pulham, C. R. (2002). *Acta Cryst.* E**58**, i79–i81.
Mark, H. & Pohland, E. (1926). *Z. Kristallogr.* **64**, 113–114.
Mayo, S. L., Olafson, B. D. & Goddard III, W. A. (1990). *J. Phys. Chem.* **94**, 8897–8909.
Merz, K. & Driess, M. (2002). *Acta Cryst.* C**58**, i101–i102.
Mirskaya, K. V. (1973). *Tetrahedron*, **29**, 679–682.
Ott, H. (1926). *Z. Kristallogr.* **63**, 222–230.
Pepe, G. & Gay, J. M. (1989). *J. Chem. Phys.* **90**, 5735–5737.
Piermarini, G. J. & Braun, A. B. (1973). *J. Phys. Chem.* **58**, 1974–1982.
Pohl, S. (1982). *Z. Kristallogr.* **159**, 211–216.
Pohland, E. (1931). *Z. Anorg. Allg. Chem.* **201**, 265–281.

Reuter, H. & Pawlak, R. (2000). *Z. Anorg. Allg. Chem.* **626**, 925–929.
Reuter, H. & Pawlak, R. (2001). *Z. Kristallogr.* **216**, 34–38.
Schmidt, M. U. (1994). *Kristallstrukturberechnungen metallorganischer Molekülverbindungen.* Aachen: Shaker.
Schmidt, M. U. & Kalkhof, H. (1997). *CRYSCA*. Frankfurt am Main, Germany.
Simon, A. & Peters, K. (1980). *Acta Cryst.* B**36**, 2750–2751.
Spitzer, R., Howell, W. J. Jr & Schomaker, V. (1943). *J. Am. Chem. Soc.* **64**, 62–67.
Varella, M. T. do N., Natalense, A. P. P., Bettega, M. H. F. & Lima, M. A. P. (1999). *Phys. Rev. A*, **60**, 3684–3693.
Walz, L., Thiery, D., Peters, E.-M., Wendel, H., Schoenherr, E. & Wojnowski, M. (1993). *Z. Kristallogr.* **216**, 207–211.
Wolf, A. K., Glinnemann, J. & Schmidt, M. U. (2008). *CrystEngComm*, **10**, 1364–1371.
Zakharov, L. N., Antipin, M. Yu., Struchkov, Yu. T., Gusev, A. V., Gibbin, A. M. & Zhernenkov, N. V. (1986). *Kristallografiya*, **31**, 171–172.